Journal of Power Sources 268 (2014) 804–809

Contents lists available at ScienceDirect

Journal of Power Sources

journal homepage: www.elsevier.com/locate/jpowsour

Chemical stability study of nanoscale thin film yttria-doped barium cerate electrolyte for micro solid oxide fuel cells

Yong Li [a], Pei-Chen Su [a, *], Lai Mun Wong [b], Shijie Wang [b]

[a] School of Mechanical and Aerospace Engineering, Nanyang Technological University, 50 Nanyang Avenue, Singapore 639798, Singapore
[b] Institute of Materials Research and Engineering, Agency for Science, Technology and Research (A*STAR), 3 Research Link, Singapore 117602, Singapore

HIGHLIGHTS

- The correlation between fuel cell performance and chemical instability BCY thin film electrolyte was revealed.
- Clear evidence of thin film cracks and mixed conducting Ce^{3+}/Ce^{4+} were observed.
- An interface-controlled decomposition mechanism for nanoscale thin film was proposed.

GRAPHICAL ABSTRACT

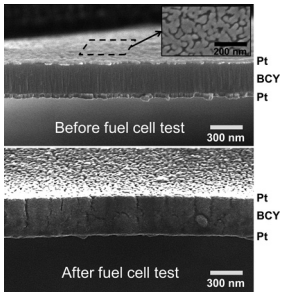

ARTICLE INFO

Article history:
Received 29 April 2014
Received in revised form
20 June 2014
Accepted 24 June 2014
Available online 7 July 2014

Keywords:
Yttria-doped barium cerate
Pulsed laser deposition
Proton-conducting ceramics
Solid oxide fuel cell
Nano thin film electrolyte

ABSTRACT

The chemical stability of a nanoscale yttria-doped barium cerate (Y–$BaCeO_3$ or BCY) thin film electrolyte for low temperature solid oxide fuel cells (SOFCs) are investigated in the temperature range of 300–400 °C. The micro-SOFCs using 300 nm-thick BCY electrolyte show a poor fuel cell performance and continuous decrease in open circuit voltage (OCV) with higher operating temperatures. Characterization results from X-ray diffraction (XRD) and X-ray photoelectron spectroscopy (XPS) revealed that the observed degrading fuel cell performance is attributed to the rapid decomposition of $BaCeO_3$ into $BaCO_3$, $Ba(OH)_2$, and CeO_2 from reactions with CO_2 and H_2O during fuel cell test. The lattice parameters of BCY expanded during fuel cell test, resulting in the formation of micro cracks along the electrolyte that possibly induced the OCV drop. The reactions of nano thin film BCY with CO_2 and H_2O are both active at temperature between 300 and 400 °C, which is unlike bulk BCY material where only the reaction with CO_2 is significant. The reduction of Ce^{4+} species into Ce^{3+} in the BCY electrolyte has also lead to an electronic conduction in BCY that lowered OCVs.

1. Introduction

Proton-conducting ceramics, such as acceptor-doped cubic perovskite-type oxides, have lower activation energies for proton transportation than conventional oxygen ion conductors and are promising electrolyte materials for SOFCs operating at temperatures below 500 °C [1–4]. In practical SOFC operation, a good chemical stability of selected electrolytes as well as a high ionic conductivity is required for long-term fuel cell operation. Currently, yttria-doped $BaZrO_3$ (BZY) and yttria-doped $BaCeO_3$ (BCY) are two of the most investigated proton-conducting ceramic electrolyte materials. BZY is known for its good proton conductivity and excellent chemical stability under fuel cell operating conditions, but the proton conductivity in practice is still relatively low due to its poor sinterability which results in high grain boundary density that blocks proton transportation [2]. On the other hand,

* Corresponding author.
E-mail addresses: peichensu@ntu.edu.sg, su.peichen@gmail.com (P.-C. Su).

http://dx.doi.org/10.1016/j.jpowsour.2014.06.128
0378-7753/

BCY has the highest ionic conductivity among all the proton-conducting ceramics [1,5]. Thin film BCY has been used to demonstrated the feasibility as a suitable electrolyte material for very low temperature (below 500 °C) SOFCs, and decent cell performance was obtained. Iijima et al. [6] coated a 2 μm-thick BCY thin film electrolyte by pulsed laser deposition (PLD) on a Pd substrate and use screen-printed $La_{0.6}Sr_{0.4}CoO_3$ and Pt as the cathode and anode. A high maximum power density of 0.9 W cm^{-2} with open circuit voltage (OCV) of over 1.0 V was obtained at 400 °C. Bae et al. [7] reported a silicon-supported micro-SOFC using nano thin film BCY with thickness of only 200 nm deposited by PLD, and a maximum power density of 145 mW cm^{-2} with an OCV of 0.98 V at 400 °C.

One major drawback of using ceria-based electrolytes is the poor chemical stability that often leads to a rapid degradation of cell performance [6,8–10]. The degradation originates from the high basicity of the electrolyte that facilitates $BaCeO_3$ to react with CO_2 and H_2O and decompose to $BaCO_3$, CeO_2, or $Ba(OH)_2$ [11–13]:

$$BaCeO_3(s) + H_2O(l) - CeO_2(s) + Ba(OH)_2(s/l) \quad (1)$$

$$BaCeO_3(s) + CO_2(g) - CeO_2(s) + BaCO_3(s) \quad (2)$$

In an effort to avoid the electrolyte decomposition, 1 μm-thick BZY was coated on a sintered bulk BCY pellets (thickness of 1 mm) to utilize its chemical stability as a protective layer against atmospheric CO_2 and moisture, and a significant improvement of performance stability was observed [14]. Similar concept was also applied to micro-SOFCs using nano thin film BCY electrolyte (thickness of 200 nm) by depositing a 20 nm-thick BZY layer on either cathode, anode, or on both sides of BCY using PLD [7]. However, the additional BZY capping layer(s) did not improve the overall chemical stability of the composite electrolyte, and rapid degradation of cell performance was still observed, possibly due to the insufficient thickness of capping layer for the nano thin film BCY. Further investigations for the behaviors of nano thin film BCY at targeted low temperature range is necessary to optimize the performance of the micro-SOFCs using this promising material.

Although the chemical stability of bulk BCY electrolyte has been well-investigated at higher temperatures [15–18], particularly for the reactions with CO_2 and H_2O [19], studies for nanoscale thin film BCY at temperatures below 500 °C are still rare due to the interests in using BCY for very low temperature SOFCs are just growing from the recent successful demonstrations [6]. In addition, most of the chemical stability analyses of cerium based proton-conducting electrolytes were performed in H_2O/CO_2 containing atmosphere or boiled water and not directly under actual fuel cell operating conditions [11–13], which may not reflect the effect of charge transport on the corrosion behaviors during fuel cell operation. Therefore, this work is dedicated as an initial study on the chemical stability of nano thin film BCY as the electrolyte for micro-SOFCs operated at very low temperature range of 300 °C–400 °C. The reactions of BCY with CO_2 and H_2O as well as the reduction of cerium after fuel cell test were identified to clarify the causes of cell performance degradation.

2. Experimental

2.1. Fabrication and test of BCY Micro-SOFCs

Fig. 1(a) shows the schematic of the silicon-based micro-SOFC with free-standing BCY electrolyte membrane fabricated using silicon micromaching processes, as previously reported in [20]. BCY thin films with thickness of 300 nm were deposited by PLD on a free-standing silicon nitride membrane supported by a silicon wafer [21]. A 248 nm KrF excimer laser (Lambda Physik) with laser fluence of 2.5 J cm^{-2} per pulse was used to ablate a sintered $BaCe_{0.9}Y_{0.1}O_{3-\delta}$ pellet target (Able Target Limited, China) with a target to substrate distance of 50 mm. The main chamber was vacuumed to a base pressure of 1×10^{-4} Pa, and the oxygen partial pressure was fixed at 1.0 Pa. After deposition, all the samples were cooled to 400 °C with a cooling rate of 10 °C min^{-1} to avoid crack formation on the membrane caused by the difference of thermal expansion coefficients between silicon substrate and the BCY membrane. The deposited films were then continued to cool to room temperature by natural convection in the chamber with same oxygen partial pressure. After the deposition of BCY electrolyte, the Si_3N_4 supporting layer was removed by relative ion etching (RIE) with CF_4 gas to obtain the free-standing BCY electrolyte. Porous Pt thin film cathode and anode with thickness of 50 nm were deposited on both sides of the electrolyte by using DC sputtering with a DC power 250 W and pressure of 80 mTorr at room temperature.

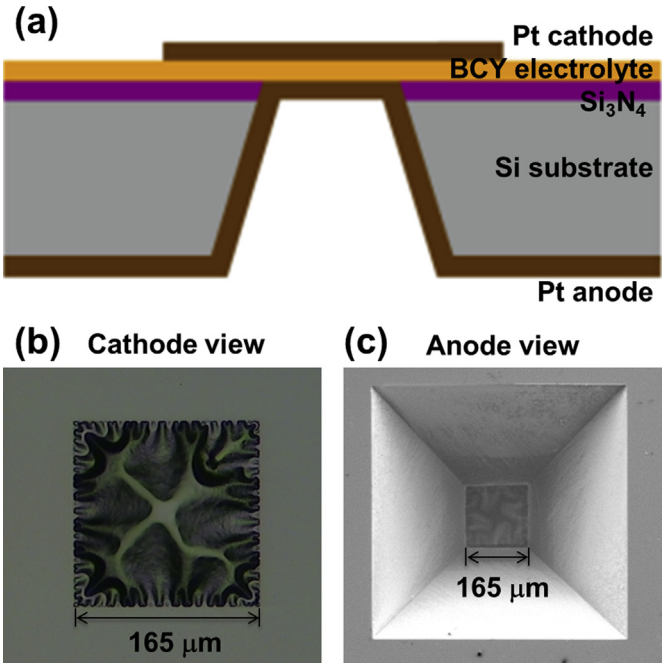

Fig. 1. Structure of free-standing micro-SOFC device. (a) Schematic of cell structure; (b) Optical microscopy image of SOFC seen from cathode side; (c) SEM image of SOFC seen from anode side.

The fuel cell performance was tested with a custom-made micro-SOFC test station as described elsewhere in [20]. The test was performed under dry hydrogen fuel at a flow rate of 20 sccm and under ambient air as oxidant, and therefore the chemical reactions between BCY and CO_2 and H_2O were with those species contained in the ambient air. The polarization curves were measured at 300, 350, and 400 °C using a potentiostat system (Solartron 1470E) and a frequency response analyzer (FRA) (Solartron 1255B).

2.2. Electrolyte characterizations

The crystallinity and structural phase of the deposited films were analyzed by Grazing incidence X-ray diffraction (GIXRD) method using a PANalytical Empyrean XRD system, with the glancing incident angle being kept at 1° for all the measurements. The collected XRD patterns were refined by the Rietveld method using the X'pert HighScore software package. The substrate Si (400) peak was used as the reference to confirm a corrected zero point for

subsequent characterizations. The composition of the BCY electrolyte and its chemical states were determined using X-ray photoelectron spectroscopy (XPS, Kratos AXIS Ultra) with a monochromatic Al Kα (1486.71 eV) X-ray radiation (15 kV/10 mA). The high-resolution spectra scans over different element peaks were recorded in a step of 0.1 eV under constant pass energy of 40 eV. The binding energies were calibrated with reference to the adventitious hydrocarbon contamination peak located at 284.8 eV. The morphologies of the electrolytes were characterized using a field-emission scanning electron microscopy (FE-SEM, JEOL JSM-7600F).

3. Results and discussion

The fabricated micro-SOFC with BCY electrolyte is shown in Fig. 1(b) and (c). The free-standing electrolyte membrane shows severe buckling, which reflected the compressive stress that was often observed in oxide thin films deposited at high temperature [22–24]. In the fuel cell polarization curves (Fig. 2), the OCVs started at a low value of 0.79 V at 300 °C, and dropped to 0.68 V at 350 °C, and finally down to 0.59 V at 400 °C. The maximum power densities were also at low values of 2, 5 and 30 mW cm^{-2} at 300, 350 and 400 °C, respectively. As shown in the SEM images of the BCY membrane cross-sectional view (Fig. 3), no noticeable crack was observed in the electrolyte before fuel cell test, and after tested at 400 °C several cracks initiated on the BCY surface and perforated across the electrolyte. The formation of such cracks could have caused gas leakage that resulted in the decreasing OCV values and the poor fuel cell power performance.

The XRD characterizations were first carried out to verify the changes of lattice parameters of BCY electrolyte (Fig. 4) before and after the fuel cell test. Both the as-deposited and tested BCY electrolytes were indexed to an orthorhombic perovskite structure (space group Pmcn), indicating that the BCY electrolyte has retained the same crystal structure after the fuel cell test. However, the XRD pattern of BCY after test shows a noisier background, and several new small peaks of $BaCO_3$ appeared after exposure to CO_2 and moisture during fuel cell test. In addition, an obvious peak shift of about 0.2° to the lower angle was observed in the tested sample, indicating an increase in the plane distance. As summarized in Table 1, the cell volume expanded from 338.01 $Å^3$ to 349.88 $Å^3$ after the fuel cell test. This volume expansion could have changed the stress level of the free-standing BCY electrolyte and resulted in the cracks we observed in the electrolyte membrane.

We further identified the chemical decomposition of BCY electrolyte by XPS. Fig. 5 shows the high-resolution spectra of Ba 3d, O 1s, C 1s, respectively. For the as deposited sample, the Ba 3d photoelectron peaks can be resolved into a set of spin-orbit doublets of Ba $3d_{5/2}$ (779.1 eV) and $3d_{3/2}$ (797.4 eV), where the peak separation of 18.3 eV is consistent with the values reported in the literature [25]. The perfectly symmetric Ba $3d_{5/2}$ peak was resolved into a single peak with Gaussian fitting, indicating that a pure $BaCeO_3$ chemical state is presented in the electrolyte. After fuel cell test at 300 °C, two small peaks formed beside the two original Ba 3d peaks with slightly higher binding energies of 779.6 eV and 797.9 eV but a same peak difference of 18.3 eV. These two new peaks indicate the formation of a new set of Ba 3d doublets (Ba $3d_{5/}$

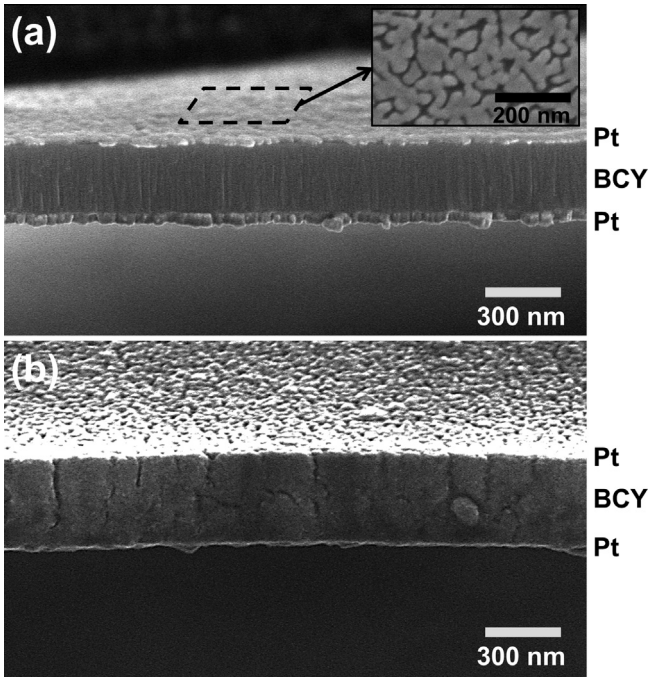

Fig. 3. Cross-sectional FE-SEM images of the BCY electrolyte before (a) and after fuel cell test at 400 °C (b). The inset figure in (a) shows a magnificent view of the porous Pt surface.

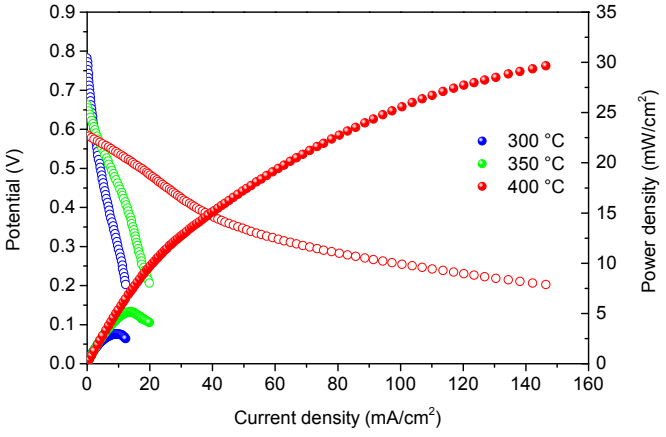

Fig. 2. Polarization curves at temperatures of 300, 350, and 400 °C.

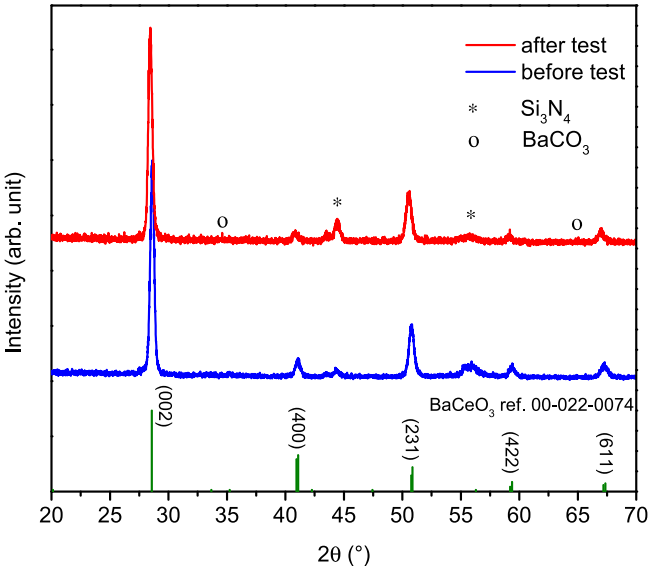

Fig. 4. Grazing incidence x-ray diffraction (GIXRD) patterns of BCY electrolyte before and after fuel cell test at 400 °C.

Table 1
Crystal structure and parameters obtained by XRD refinement.

	2θ (°)	d-spacing (Å)	a (Å)	b (Å)	c (Å)	Volume (Å^3)
Before	28.585	3.12023	8.7529	6.1914	6.2371	338.01
After	28.435	3.13635	8.9426	6.2334	6.2767	349.88

$_2$ and $3d_{3/2}$), which corresponds to a different barium binding state that can be resolved to $Ba(OH)_2$ as indexed to reference [26]. As the testing temperature was increased to 400 °C, the intensities of these two additional peaks increased further. Similar trend was also observed in the O 1s spectra, as shown in Fig. 5(b). The O 1s XPS spectra show broad and asymmetric peaks and can be fitted to three overlapped peaks with binding energy in the region of 528–534 eV. The fitted peaks located at 530.9, 528.8, 532.2 eV were resolved to lattice oxygen, metal oxide and absorbed oxygen, respectively. For the tested sample, another O 1s peak formed at higher binding energy (~534 eV), which is also identified to associate with the formation of $Ba(OH)_2$. The C 1s spectra are also deconvoluted and shown in Fig. 5(c) for comparison. The concentration of C 1s spectra almost kept constant except a slight increase at 400 °C, indicating a much more stable carbon oxidation state than Ba after fuel cell test. Therefore, we can confirm that the newly formed Ba peaks are mainly attributed to the formation of $Ba(OH)_2$ from the electrolyte reaction with moistures. Previous researches reported that barium cerate reacts more easily with CO_2 than with water vapor, and the reaction with H_2O is not significant at the fuel cell operating conditions (400–700 °C) [14,27]. From our results, however, the analysis of Ba 3d, O 1s and C 1s XPS spectra shows the reaction with water to form $Ba(OH)_2$ is also significant and contributes to the degradation of nano thin film BCY at temperatures below 400 °C.

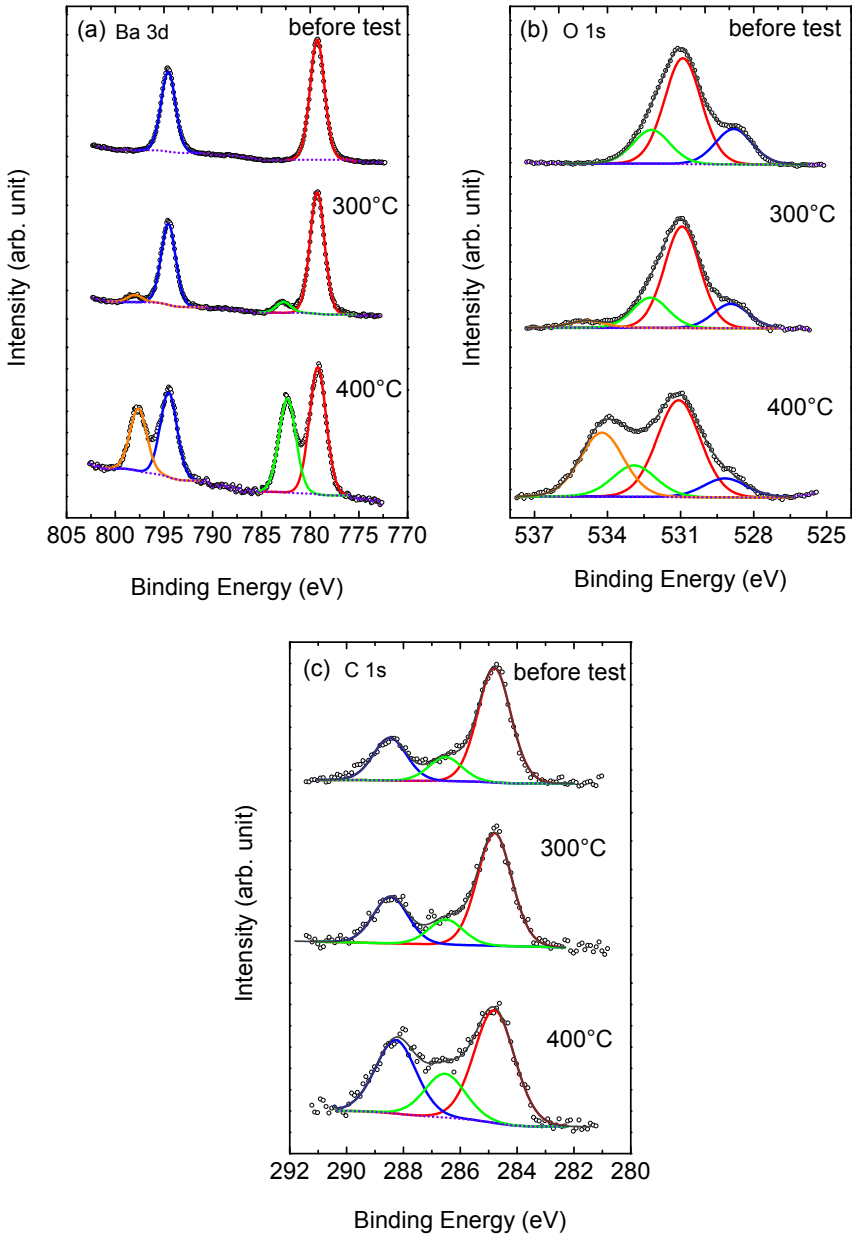

Fig. 5. XPS spectra of Ba 3d (a), C 1s (b) and O 1s (c) for the BCY electrolyte before (top) and after fuel cell tested at 300 (middle) and 400 °C (bottom). The original data, fitted spectra and Shirley background are shown in hollow points, colored solid lines and dotted line, respectively.

The oxidation state of cerium is another important indicator for the poor chemical stability of nano thin film BCY electrolyte under low temperature fuel cell operating conditions. The change in oxidation state of cerium can be observed by analyzing Ce 3d spectra, as shown in Fig. 6. Due to shake-up, shake-down and multiplet splitting effects, the shape of the Ce 3d spectra contains contributions from many components, leading to complex fine structure curve fittings [28,29]. Both of the Ce 3d spectra can be resolved into 11 peaks, as illustrated with different colors. Ten cerium peaks following the notation defined by Burroughs et al. [30] using (u,v)s are attributed to the two spin-orbit split components of the Ce 3d photoemission process: the Ce $3d_{5/2}$ and Ce $3d_{3/2}$. An Auger line of barium appears in this energy range, which is colored with purple. All the Ce 3d spin-orbit splitting are in the range of 18.2–18.6 eV, which is consistent with data previously reported in the literature [31]. The core level binding energies and atomic compositions of Ce 3d doublets peaks (uv)s are calculated and summarized in Table 2 following Romeo et al.'s method [32], which is a simple and accurate way to analyze the complexity of Ce 3d spectra. The fitted curves are classified into two different sets of Ce 3d status according to their binding energies. Previous studies have confirmed that the doublets peaks, $u'''v'''$, $u''v''$, uv are originated from Ce^{4+} oxidation state, and $u'v'$ and u_0v_0 are attributed to the Ce^{3+} oxidation state [32]. As shown in Fig. 6, peaks $u'v'$, u_0v_0 are presented in both the untested and tested samples, meaning that Ce^{3+} have already existed in the BCY electrolytes before the fuel cell test, which is not expected in the fully oxidized BCY electrolyte. We speculate that the observed Ce^{3+} is present at the electrolyte surface that was exposed to ambient air that facilitates the reduction. Another possible reason may be from the X-ray induced photo reduction of cerium based samples during XPS test, though the mechanism is in principle known but not entirely understood [33]. The shape of the highest binding energy peak pair u''' and v''' (at 915 eV and 897 eV), which can be indexed to CeO_2 spectra [28,32], gives a larger enclosed area under the peaks as compared with the untested sample. The formation of CeO_2 during the fuel cell test gives a direct evidence of both reactions with CO_2 and water vapor. On the other hand, the components of Ce^{4+} $u''v''$ and uv have dramatically decreased compared with the fresh samples, especially for $u''v''$ peaks. This decrease is attributed to the partial reduction of Ce^{4+} into Ce^{3+} species, which can be confirmed by the noticeable increase in $u'v'$ and u_0v_0 peaks in the tested sample. Particularly, for the peaks of u_0v_0, the calculated concentration has increased from 9.65% to 28.35%. Considering all the oxidation states of Ce elements in the BCY electrolyte, the ratio of Ce^{3+}/Ce^{4+} has increased from 31.25% to 47.14% after fuel cell test. The co-existence of both valence states is attributed to the partial reduction of Ce (from Ce^{4+} to Ce^{3+}) [34]. Since the transformation of Ce valence state has a strong influence on the mechanical properties of Ce-based oxides [35], the large amount of Ce reduction can be associated with the lattice expansion observed from our XRD results. Such lattice expansion in a bulk BCY may not be directly visible and the effect was reflected as impact on the mechanical property, but in nano thin film BCY the lattice expansion can have directly resulted in visible cracks as we observed. Further investigation is necessary to find out the actual correlation between the changes in Ce oxidation state and the fracture of the nanoscale thin film BCY. Earlier work has shown that the existence of mixed Ce^{4+}/Ce^{3+} valence state in the CeO_2-electrolyte can provide electronic conduction through the electron hopping-transport mechanism between Ce^{4+} and Ce^{3+} [36]. For oxygen ion conductors, the ionic conduction is dominant at lower temperature range in CeO_2-based electrolytes, and at higher SOFC operating temperature (>600 °C) the electronic conductivity becomes comparable to or eventually greater than the ionic conductivity [37,38]. We also speculate the existence of electronic conduction due to the presence of CeO_2 and mixed Ce^{4+}/Ce^{3+}, which would result in the low OCVs.

Table 2
Fitted curves and calculated concentration of the characteristic XPS lines for Ce^{4+} and Ce^{3+}.

Oxidation states	Peak	Before test			After test (400 °C)		
		Position (eV)	% Concentration		Position (eV)	% Concentration	
Ce (IV)	u'''	914.86	9.91	68.75	915.36	11.52	52.86
	v'''	896.56	10.37		897.09	12.06	
	u''	908.50	12.26		907.99	5.70	
	v''	890.20	12.84		889.39	5.95	
	u	903.00	11.42		902.89	8.61	
	v	884.40	11.95		884.41	9.02	
Ce (III)	u'	905.98	10.55	31.25	905.18	9.18	47.14
	v'	887.78	11.05		887.04	9.61	
	u_0	899.59	4.71		900.04	13.85	
	v_0	881.29	4.94		881.45	14.5	

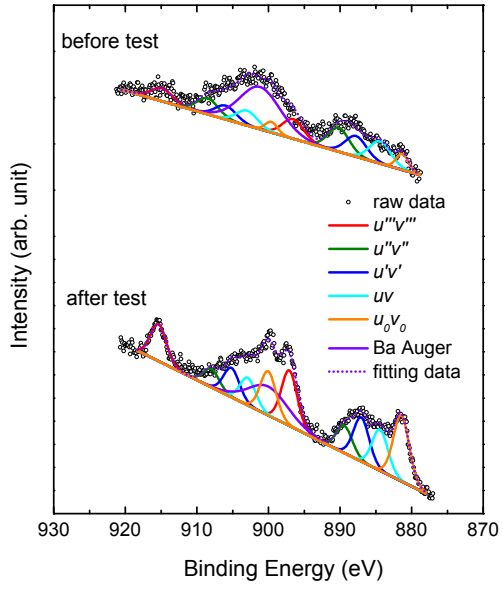

Fig. 6. XPS spectra of Ce 3d for the BCY electrolyte before and after fuel cell test at 400 °C.

In addition, the chemical stability of our nano thin film BCY electrolyte can be more vulnerable to reduction to Ce^{3+} than bulk BCY under fuel cell operating conditions due to a higher surface-to-volume ratio, which increases the relative exposure to CO_2 and H_2O. We noticed that most of the cracks in the electrolyte initiated from the cathode surface (Fig. 3(b)), possibly due to the water vapor produced at the cathode side during fuel cell operation and promoted the reaction in Equation (1). It is reported that in the presence of moisture in the environment, the decomposition kinetic of $BaCeO_3$ is controlled by the diffusion of water into the perovskite lattice [12]. In our case of nano thin film electrolyte, since the diffusion pathway is much shorter than that in a bulk electrolyte, the decomposition kinetics is controlled by the contact interface between the BCY electrolyte and moisture environment, as seen from SEM images that the cracks seem to propagate from the electrolyte surface to the center. The possible decomposition mechanism of thin film BCY electrolyte can be understood as an interface-controlled process: the gaseous reactants are in contact with BCY surface and the corrosion reactions (1) and (2) occur. The products, $BaCO_3$, $Ba(OH)_2$ and CeO_2 formed at electrolyte surface,

changed the intrinsic stress level of the pristine free-standing BCY thin film (shown in XRD analysis, Fig. 4 and Table 1), resulting in cracks formation at the surface. The decomposition of BCY did not occur over the entire surface but only at certain spots to form the cracks due to the partial coverage of surface by porous Pt electrode to block the exposure to water and CO_2. The nanoscale thickness of BCY electrolyte could have accelerated the corrosion processes. Thus, the intrinsic instability of ceria-based BCY electrolyte, together with the higher relative exposed surface area of a nano thin film, has rapidly deteriorated the fuel cell performance of BCY micro-SOFCs.

4. Conclusion

In this work, we have gained direct evidence of the chemical instability of nanoscale BCY thin film as an electrolyte for micro-SOFCs. The micro-SOFC showed a decreasing OCV with increasing operating temperature due to the chemical instability in fuel cell operating environments. Visible vertical cracks were induced from reactions with CO_2 and H_2O vapor that expanded the BCY lattice, leading to an insufficient gas separation of fuels and air. Unlike bulk BCY at high temperatures where only the reaction with CO_2 is significant, the reactions of nano thin film BCY with CO_2 and H_2O are both active at temperature between 300 and 400 °C. The reduction of Ce^{4+} into Ce^{3+} in BCY induced the electronic conduction that also resulted in the decrease of OCV. For future utilization of nanoscale BCY thin film electrolyte for low temperature micro-SOFCs, an effective way to enhance the chemical stability of BCY is necessary.

Acknowledgment

The authors would like to thank the financial support by Tier 1 Grant (No. RG 53/11) from Singapore Ministry of Education and the National Research Foundation (NRF), Prime Minister's Office, Singapore under its Campus for Research Excellence and Technological Enterprise (CREATE) programme.

References

[1] K.D. Kreuer, Annu. Rev. Mater. Res. 33 (2003) 333–359.
[2] E. Fabbri, D. Pergolesi, E. Traversa, Chem. Soc. Rev. 39 (2010) 4355–4369.
[3] E. Fabbri, L. Bi, D. Pergolesi, E. Traversa, Adv. Mater. 24 (2012) 195–208.
[4] S. Ha, P.-C. Su, S. Ji, S.W. Cha, Thin Solid Films 544 (2013) 125–128.
[5] T. Hibino, A. Hashimoto, M. Suzuki, M. Sano, J. Phys. Chem. B 105 (2001) 11399–11401.
[6] M. Iijima, N. Ito, S. Matsumoto, S. Iguchi, MRS Proc. 972 (2007).
[7] K. Bae, D.Y. Jang, H.J. Jung, J.W. Kim, J.-W. Son, J.H. Shim, J. Power Sources 248 (2014) 1163–1169.
[8] R. Kannan, K. Singh, S. Gill, T. Furstenhaupt, V. Thangadurai, Sci. Rep. 3 (2013) 2138.
[9] W. Zając, D. Rusinek, K. Zheng, J. Molenda, Cent. Eur. J. Chem. 11 (2012) 471–484.
[10] E. Fabbri, A. Depifanio, E. Dibartolomeo, S. Licoccia, E. Traversa, Solid State Ion 179 (2008) 558–564.
[11] C.W. Tanner, A.V. Virkar, J. Electrochem. Soc. 143 (1996) 1386–1389.
[12] S.V. Bhide, A.V. Virkar, J. Electrochem. Soc. 146 (1999) 2038–2044.
[13] K. Takeuchi, C.K. Loong, J.W. Richardson, J. Guan, S.E. Dorris, U. Balachandran, Solid State Ionics 138 (2000) 63–77.
[14] E. Fabbri, D. Pergolesi, A. D'Epifanio, E. Di Bartolomeo, G. Balestrino, S. Licoccia, E. Traversa, Energy Environ. Sci. 1 (2008) 355.
[15] L. Bi, S.Q. Zhang, L. Zhang, Z.T. Tao, H.Q. Wang, W. Liu, Int. J. Hydrogen Energy 34 (2009) 2421–2425.
[16] K. Xie, R.Q. Yan, X.R. Chen, D.H. Dong, S.L. Wang, X.Q. Liu, G.Y. Meng, J. Alloys Compd. 472 (2009) 551–555.
[17] J.M. Serra, W.A. Meulenberg, J. Am. Ceram. Soc. 90 (2007) 2082–2089.
[18] Z.T. Tao, Z.W. Zhu, H.Q. Wang, W. Liu, J. Power Sources 195 (2010) 3481–3484.
[19] J. Dauter, N. Maffei, S.S. Bhella, V. Thangadurai, J. Electrochem. Soc. 157 (2010) B1413–B1418.
[20] H. Huang, M. Nakamura, P.C. Su, R. Fasching, Y. Saito, F.B. Prinz, J. Electrochem. Soc. 154 (2007) B20–B24.
[21] P.-C. Su, F.B. Prinz, Microelectron. Eng. 88 (2011) 2405–2407.
[22] Y. Takagi, B.K. Lai, K. Kerman, S. Ramanathan, Energy Environ. Sci. 4 (2011) 3473–3478.
[23] K. Kerman, B.K. Lai, S. Ramanathan, J. Power Sources 196 (2011) 2608–2614.
[24] Y. Takagi, K. Kerman, C. Ko, S. Ramanathan, J. Power Sources 243 (2013) 1–9.
[25] L.L. Jiang, X.G. Tang, S.J. Kuang, H.F. Xiong, Appl. Surf. Sci. 255 (2009) 8913–8916.
[26] A.V. Fetisov, G.A. Kozhina, S.K. Estemirova, V.B. Fetisov, V.Y. Mitrofanov, S.A. Uporov, L.B. Vedmid, J. Spectrosc. 2013 (2013) 1–13.
[27] S.M. Haile, G. Staneff, K.H. Ryu, J. Mater. Sci. 36 (2001) 1149–1160.
[28] A. Trovarelli, G. Dolcetti, C. Deleitenburg, J. Kaspar, P. Finetti, A. Santoni, J. Chem. Soc. Faraday T 88 (1992) 1311–1319.
[29] J. Li, U.G. Singh, J.W. Bennett, K. Page, J.C. Weaver, J.-P. Zhang, T. Proffen, A.M. Rappe, S. Scott, R. Seshadri, Chem. Mater. 19 (2007) 1418–1426.
[30] P. Burroughs, A. Hamnett, A.F. Orchard, G. Thornton, J. Chem. Soc. Dalt. Trans. (1976) 1686.
[31] E. Bêche, P. Charvin, D. Perarnau, S. Abanades, G. Flamant, Surf. Interface Analysis 40 (2008) 264–267.
[32] M. Romeo, K. Bak, J. Elfallah, F. Lenormand, L. Hilaire, Surf. Interface Analysis 20 (1993) 508–512.
[33] E. Paparazzo, G.M. Ingo, J. Electron Spectrosc. Relat. Phenom. 95 (1998) 301–304.
[34] T.-N. Lin, M.-C. Lee, R.-J. Yang, J.-C. Chang, W.-X. Kao, L.-S. Lee, Mater. Lett. 81 (2012) 185–188.
[35] H.J. Ko, J.J. Lee, S.-H. Hyun, Electrochem. Solid State Lett. (2009) 1611–1616.
[36] T. Otake, H. Yugami, H. Naito, K. Kawamura, T. Kawada, J. Mizusaki, Solid State Ion 135 (2000) 663–667.
[37] M. Mogensen, N.M. Sammes, G.A. Tompsett, Solid State Ion 129 (2000) 63–94.
[38] M. Chen, B.H. Kim, Q. Xu, B.K. Ahn, W.J. Kang, D.P. Huang, Ceram. Int. 35 (2009) 1335–1343.